ELSEVIER

Journal of Nuclear Materials 312 (2003) 103–110

journal of nuclear materials

www.elsevier.com/locate/jnucmat

A XAS study of the local environments of cations in (U, Ce)O_2

Philippe Martin [a,*], Michel Ripert [a], Thierry Petit [a], Tobias Reich [b], Christoph Hennig [b], Francesco D'Acapito [c], Jean Louis Hazemann [d], Olivier Proux [d]

[a] CEA-Cadarache, DEN/DEC/SESC/LLCC, Bâtiment 315, 13108 Saint-Paul lez Durance cedex, France
[b] Institute of Radiochemistry, Forschungszentrum Rossendorf, P.O. Box 510119, 01314 Dresden, Germany
[c] GILDA/CRG – ESRF 6, Rue Jules Horowitz, B.P. 220, F-38043 Grenoble, France
[d] CNRS – Laboratoire de Cristallographie, BP 166, 38042 Grenoble cedex 09, France

Received 16 October 2002; accepted 5 November 2002

Abstract

Mixed oxide (MOX) fuel is usually considered as a solid solution formed by uranium and plutonium dioxides. Nevertheless, some physico-chemical properties of (U_{1-y}, Pu_y)O_2 samples manufactured under industrial conditions showed anomalies in the domain of plutonium contents ranging between 3 and 15 at.%. Cerium is commonly used as an inactive analogue of plutonium in preliminary studies on MOX fuels. Extended X-ray Absorption Fine Structure (EXAFS) measurements performed at the European Synchrotron Radiation Facility (ESRF) at the cerium and uranium edges on (U_{1-y}, Ce_y)O_2 samples are presented and discussed. They confirmed on an atomic scale the formation of an ideal solid solution for cerium concentrations ranging between 0 and 50 at.%.

PACS: 61.10.Ht; 64.75.+g; 28.41.Bm

1. Introduction

Mixed oxide (MOX) fuel is usually considered as a solid solution formed by uranium and plutonium dioxides. Nevertheless for (U_{1-y}, Pu_y)O_2 samples manufactured under industrial conditions, Beauvy [1] highlighted anomalies of some physico-chemical properties for samples with plutonium contents ranging between 3 and 15 at.%.

Cerium is commonly used as an inactive analogue to plutonium in preliminary studies on MOX fuels. Indeed, the ionic radius of this element and its chemical properties connected to its 4f electrons are very close to the ones observed for plutonium. Moreover, cerium and uranium dioxides are known to form a solid solution [2,3].

The X-ray Absorption Spectroscopy (XAS) is very sensitive to short range order around the absorbing atom and seems to be the ideal technique to probe the local environments of the cations forming the solid solution. Indeed, this technique is usually used to check the random substitution of the elements forming a solid solution [4]. To our knowledge, very few studies using synchrotron radiation were applied to nuclear fuel analysis. Jones et al. [5] showed that the presence of defects due to non-stoichiometry is easily characterized by this technique. More recently, the study of the oxygen absorption K-edge [6,7] has contributed to furthering our understanding of the electronic structure of uranium dioxide.

In the present paper, as a first step, we propose to highlight the benefits of XAS to characterise (U_{1-y}, Ce_y)O_2 samples ($0 < y < 0.5$) and to confirm on an atomic scale the formation of a solid solution. After a

* Corresponding author. Tel.: +33-4 4225 3866; fax: +33-4 4225 3713.
E-mail address: martinp@drncad.cea.fr (P. Martin).

0022-3115/03/$ - see front matter
PII: S0022-3115(02)01590-8

description of the experimental conditions and the fitting procedures, the results obtained are presented and discussed.

2. Experimental details

The UO_2, CeO_2 and $(U_{1-y}, Ce_y)O_2$ pellet samples used in the current study were supplied by the Société Industrielle du Combustible Nucléaire. The UO_2 and CeO_2 powders are milled together in a ball-mill to obtain a homogeneous mixing of both powders. The powder is then compacted in a rotating press to form thin disks, which are crushed and sieved to elaborate granulated powder. The main goal of this granulation stage is to facilitate the press die filling. After pressing and sintering in a hydrogen atmosphere during about 4 h at 1700 °C, the size of the pellets is about 8 mm in diameter and 1 mm thickness. The average weight of each pellet is about 600 mg leading to activities lower than 370 kBq by sample. They can thus be easily imported on any beam line in sealed polyethylene bags. The $(U_{1-y}, Ce_y)O_2$ selected compositions are: $y = 5$, 10, 12, 18, 25 and 50 at.% of cerium.

The Extended X-ray Absorption Fine Structure (EXAFS) spectroscopy was carried out at the European Synchrotron Radiation Facility (ESRF) storage ring in Grenoble, on three different beam lines.

The first set of scans was collected on the BM20 Rossendorf BeamLine (ROBL) [8]. During this session, the uranium L_{III} edge EXAFS spectra of UO_2 and $(U_{1-y}, Ce_y)O_2$ were recorded at room temperature in fluorescence mode. The sample surface was oriented 45 degrees to both the beam direction and the window of the Ge solid state detector. We also tried to collect data at the cerium L_{III} and L_I edges. No significant information was obtained at the cerium L_{III} edge because of the narrow energy interval (between 5723 and 6165 eV, the cerium L_{III} and L_{II} edges, respectively). The signal to noise ratio was not good enough to perform a detailed quantitative analysis. This behaviour can be explained by the occurrence of the double electron excitation [9], the detection mode, and the low amount of cerium in the samples. The uranium M_I edge (5548 eV), 200 eV below the cerium L_{III} edge also deteriorates the spectra. As Fonda et al. [9] have demonstrated, the double electron excitation is avoided at the cerium L_I edge but only the higher cerium concentrations (25 and 50 at.%) give accurate spectra.

The second measurement campaign was made at the BM 32 InterFaces (IF) beam line at the uranium L_{III} edge. These experiments were also carried out in the fluorescence mode at room temperature. Measurement of the fluorescence yield was performed using a 30-element solid germanium Canberra energy-resolved detector. The monochromator was a (1 1 1) Si 2-crystals in order to have a maximum flux on the sample. Moreover, the dynamical bending of the second crystal of the monochromator allows to focus the beam in the horizontal plane. This focalisation process is necessary, the horizontal divergence of the beam being rather large on a bending magnet. Without loosing flux, the size of the X-ray spot on the sample is then around 0.3 by 0.3 mm^2, smaller than the pellets size.

For our proposal to study the cerium environment at low cerium concentration, some beam time was also allocated at the BM 8 General purpose Italian Line for Diffraction and Absorption (GILDA) beam line at the cerium K-edge. The monochromator was equipped with a curved (5 1 1) Si crystal and run in a dynamical focusing mode [10]. To obtain better quality spectra, all the data were collected at liquid nitrogen temperature. The X-ray absorption spectrum of cerium dioxide CeO_2 was collected in transmission mode, using ionisation chambers filled with argon gas. The $(U_{0.95}, Ce_{0.05})O_2$ and $(U_{0.90}, Ce_{0.10})O_2$ were recorded between 40 000 and 42 000 eV in fluorescence detection mode, using a 13-element Ge detector. Energy calibration for the Ce K-edge was performed by assigning the first inflexion point in the absorption edge of CeO_2 to 40 445 eV.

3. Analysis details

The space group of cerium and uranium dioxides is $Fm\bar{3}m$ with a cell parameter a of 5.411 and 5.470 Å, respectively. The atomic coordinates in the unit cell are metal at $(0, 0, 0)$ and oxygen at $(0.25, 0.25, 0.25)$. In the structure, we can identify successive coordination shells around the metal atom. Data referring to the first four shells are reported in Table 1.

In the case of an ideal solid solution $(U_{1-y}, Ce_y)O_2$, the lattice parameter follows the Vegard's law. Yamada et al. [11] showed this behaviour and gave the following relationship between the lattice parameter a in angstroms and the cerium content y:

$$a = 5.47(1 - 1.14 \times 10^{-2} y). \quad (1)$$

Table 1
Structure of the first four atomic shells around a metal atom in CeO_2 and UO_2

Shell number	Atom	Coordination number	Distance in CeO_2 (Å)	Distance in UO_2 (Å)
1	O	8	2.343	2.369
2	Ce or U	12	3.826	3.868
3	O	24	4.487	4.535
4	Ce or U	6	5.411	5.470

Table 2
Evolution of the three first shell distances as a function of cerium concentration in $(U_{1-y}, Ce_y)O_2$

Cerium concentration (at.%)	Lattice parameter (Å)	Metal–oxygen distance (Å) first shell	Metal–metal distance (Å) second shell	Metal–oxygen distance (Å) third shell
5	5.467	2.367	3.866	4.533
10	5.464	2.366	3.863	4.530
12	5.463	2.365	3.863	4.529
18	5.459	2.364	3.860	4.526
25	5.454	2.362	3.857	4.523
50	5.439	2.355	3.846	4.510

Numerical values for the distances corresponding to the first three coordination shells are derived based on crystallographic considerations from this expression of the lattice parameter. They are gathered in Table 2.

At least four scans were collected at each edge. For the $(U_{1-y}, Ce_y)O_2$ spectra, because of the high concentration of the probed elements, the experimental signals were systematically underestimated. Indeed, since the amount of the probed atom is higher than 5 at.%, a reabsorption process of part of the fluorescence signal occurs. This phenomenon is well known and was quantified by Tröger et al. [12]. In our case, the amplitude of the experimental EXAFS oscillations were corrected using the FLUO program (part of the UWXAFS 3.0 package [13]), which is precisely based on Tröger's work [12].

For this correction to be possible, we supposed that our samples are homogeneous all along the mean photon path. In order to validate this program, we also have to compare the results obtained by dividing the extracted UO_2 EXAFS signal by 0.69, this value was calculated by the algorithms described by Tröger et al. We obtained the same results with the two methods.

The fine structure oscillations are isolated from the raw absorption spectra using the AUTOBK program [13]. The background is approximated using a polynomial spline function with knots through the post-edge region. The values of the spline at the knot energies are found to minimise the integrated intensity in the Fourier transform moduli of the EXAFS between 0 and R_{bkg}. The values of the parameter R_{bkg} were ranging between 1.1 and 1.6 Å, depending on the element and edge.

For the EXAFS data analysis, we used the FEFFIT software [14]. Theoretical scattering amplitudes and phases were calculated with the FEFF8.10 program [15]. During the fit of the reference compounds UO_2 and CeO_2, the number of atoms for each coordination shell was kept constant at their theoretical values. Due to the high quality of the spectra, we used k^3-weighting for all uranium EXAFS signals during the fitting process. On the opposite, all the scans collected at cerium L_I and K-edges were only k^2-weighted.

4. Reference compounds

Fig. 1(a) shows the XAFS pseudo radial distribution function (RDF) modulus obtained after Fourier Transform of the UO_2 reference sample spectrum over the k-space range 3.0–14.5 Å^{-1}. This RDF is characterised, in apparent distances, by two peaks located at around 2 and 4 Å. As described in Table 1, they correspond to the three first distances U–O (2.369 Å), U–U (3.868 Å) and U–O (4.535 Å). Because of the big difference between the atomic number of the two elements, the contributions of the second and third distances merged in the Fourier Transform. The limits of the domain considered are situated between 1.35 and 4.2 Å as represented in Fig. 1(a) by the two arrows. The EXAFS signal obtained by reverse transformation in this domain is shown in Fig. 1(b).

We checked the number of scattering paths needed to obtain a good simulation of the EXAFS signal and the best agreement between structural parameters calculated by FEFF8.10 and crystallographic data.

We first introduced into the simulation, the single scattering contributions due to the first three shells of atomic neighbours. All the results are gathered in Fig. 1 and Table 3. The agreement between experimental and simulated data is fairly good as shown by a R-factor of 0.015, which means that theory and data agree within 1.5%. The interatomic distances determined by EXAFS measurements are very close to that calculated using lattice constants and crystallographic coordinates.

Then, we took into account the effect of multiple scattering. We only considered in our calculations the major scattering paths given by FEFF8.10 calculation, by selecting the paths whose amplitude has a weight greater than 7% of the first coordination shell and a maximum length of 5 Å. Accordingly, the two new paths considered are the following ones:

U–O–O (degeneracy = 48, $R = 4.8195$ Å, weight = 13%),
U–O–U–O (degeneracy = 8, $R = 4.737$ Å, weight = 15%).

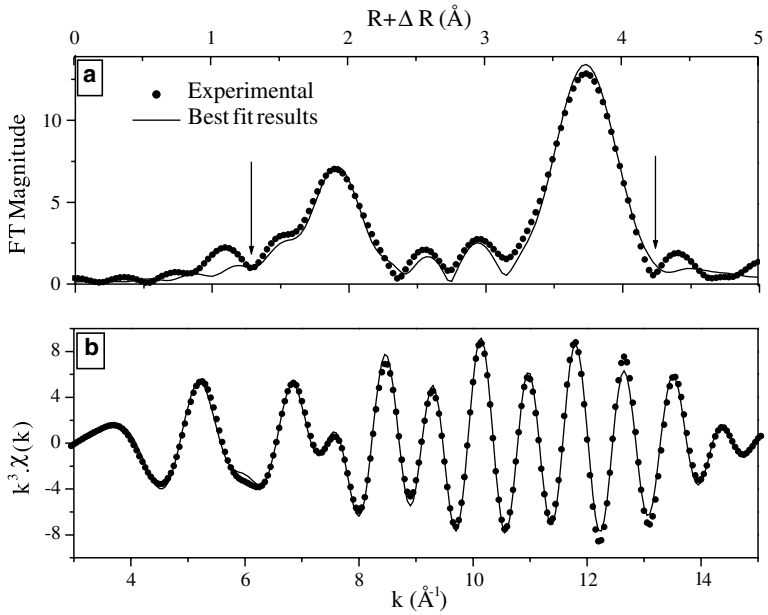

Fig. 1. Uranium L_{III} edge k^3-weighted EXAFS data (b) including the best fit and corresponding FT (a) for UO_2. The two arrows indicate the fit limits.

Table 3
Best fit results for reference compounds relative to the first three coordination shells obtained at the uranium L_{III} edge for UO_2 and cerium K-edge for CeO_2

Shell description	Coordination number	Distance (Å)	σ^2 (Å^2)
UO_2			
U–O	8	2.372(5)	0.0072(6)
U–U	12	3.87(1)	0.0039(1)
U–O	24	4.52(1)	0.007(1)
ΔE_0 (eV)	0.9(5)		
R factor	0.015		
CeO_2			
Ce–O	8	2.338(7)	0.0045(4)
Ce–Ce	12	3.83(1)	0.0022(3)
Ce–O	24	4.48(2)	0.006(2)
ΔE_0 (eV)	1.8(5)		
R factor	0.005		

In the *k*-range determined in the first fit, the fitting procedure leads to same values for the three first coordination shells. The *R*-factor of the fit becomes lower than 1%. The improvement thus caused by the addition of multiple scattering paths is negligible in comparison with the number of independent parameters to be determined in the refinement. On this basis, no multiple scattering path will be considered in the fits of $(U_{1-y}, Ce_y)O_2$ scans collected at the uranium L_{III} edge.

The same methodology was employed for the analysis of the other reference compound, CeO_2. Fig. 2(a) shows the RDF modulus obtained after Fourier transform of the CeO_2 spectrum in the *k*-range 3.0–18.0 Å^{-1}. The interval used for the fits is represented in Fig. 2(a) by two arrows.

As observed in the case of UO_2, this spectrum exhibits the signature of cubic symmetry: two main peaks localised at around 2 and 3.5 Å. The EXAFS signal obtained by reverse transformation is presented in Fig. 2(b), while the numerical values of the fits are given in Table 3. These values are very close to the crystallographic ones. The addition of the main multiple scattering paths only induces a slightly improvement of the refinement, and will not be introduced into the next fits at the cerium edges. It is interesting to point out that Fonda et al. [9] came to the same conclusion.

5. $(U_{1-y}, Ce_y)O_2$ samples

For each sample, theoretical scattering amplitudes and phases were calculated with FEFF8.10 using cell parameters calculated with Eq. (1).

In Fig. 3, we can see the evolution of the RDF from UO_2 to $(U_{0.5}, Ce_{0.5})O_2$. The intensity of the peak corresponding to the uranium–metal shell decreases as the cerium content rises. No major modification is noticeable on the first peak. Whatever the cerium content is, the crystallographic structure appears to be face centred

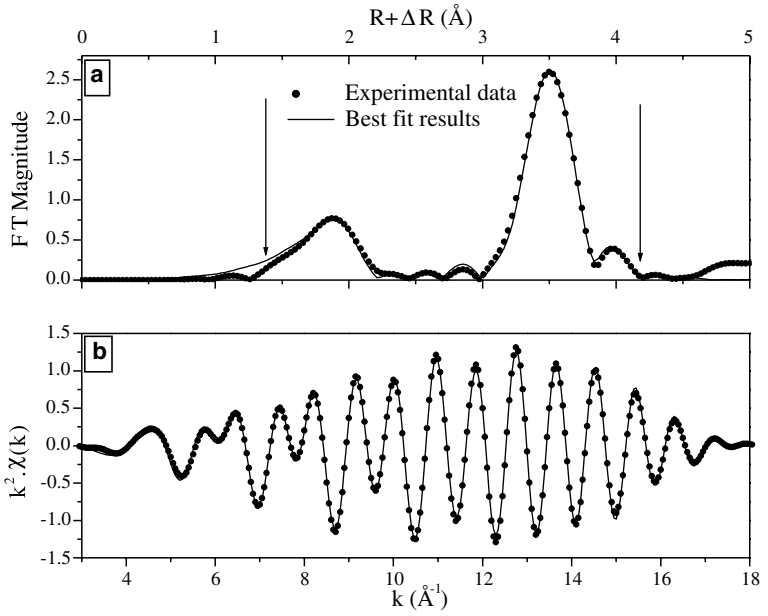

Fig. 2. Cerium K-edge k^2-weighted EXAFS data (b) including the best fit and corresponding FT (a) for CeO_2. The two arrows indicate the fit limits.

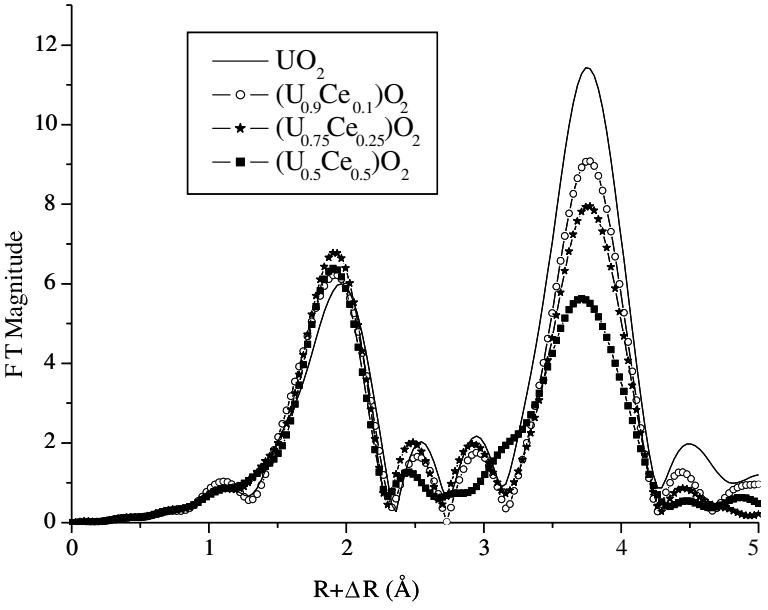

Fig. 3. Change as a function of the cerium content of the RDF at the uranium L_{III} edge. (The FT window is taken over the k-space range 3.0 and 14.5 $Å^{-1}$ and magnified by k^3.)

cubic. All the compounds were fitted between 1.3 and 4.2 Å. The results are gathered in Tables 4 and 5.

The first evidence of the formation of a solid solution is clearly seen in the coordination numbers N for the metal–metal shells. At both metal edges, the fit gives the theoretical values for each Ce concentration. For instance, N is equal to 6.0 ± 0.3 for the 50 at.% sample at both the uranium and cerium edges. This observation

Table 4
ΔE_0 and R-factor values obtained for the whole $(U_{1-y}, Ce_y)O_2$ EXAFS refinements

Sample	Edge	ΔE_0 (eV)	R factor
$(U_{0.95}, Ce_{0.05})O_2$	Uranium L_{III}	0.6(5)	0.008
	Cerium K	1.8(5)	0.013
$(U_{0.90}, Ce_{0.10})O_2$	Uranium L_{III}	0.8(5)	0.012
	Cerium K	0.1(5)	0.017
$(U_{0.88}, Ce_{0.12})O_2$	Uranium L_{III}	3.7(5)	0.014
$(U_{0.82}, Ce_{0.18})O_2$	Uranium L_{III}	3.7(5)	0.014
$(U_{0.75}, Ce_{0.25})O_2$	Uranium L_{III}	2.1(6)	0.012
$(U_{0.50}, Ce_{0.50})O_2$	Uranium L_{III}	1.7(6)	0.012
	Cerium L_I	−14.6(6)	0.020

seems to indicate that the metal ions are randomly distributed in the cationic site of the $Fm\bar{3}m$ lattice as expected in a solid solution.

Furthermore, the fact that N remains equal to 8.0 ± 0.2 and 24 ± 2 for the first and third shells indicates that oxygen stoichiometry is well maintained in all the cases. Moreover, as the RDF shows, the apparent distances decrease with the increase of cerium content as expected in the Table 2.

The values obtained at the cerium K-edge are gathered in Table 6. It should be noted that, at this edge, the addition of the cerium–cerium distance in the second coordination shell does not improve the overall quality of the fits. Indeed the cerium–metal distance and its Debye–Waller factors remain unchanged in the experimental error margin. At first sight, this result is quite surprising, but a closer examination of the EXAFS signals of the two cerium–cerium and cerium–uranium scattering paths calculated by FEFF shows that they are in total phase opposition. Moreover, uranium has a much higher amplitude than cerium alone. This observation explains why for low cerium contents, which are the subject of this article, the metal–metal coordination shell is perfectly simulated by the first cerium–metal path. We plotted in Figs. 4 and 5 the distances determined for the two atoms probed in the first and second coordination shells. We can see in both cases, that all the values are in agreement with the Vegard's law.

6. Discussion

As we just said, for all the samples studied, the Vegard's law is obeyed. This implies the following observations.

The industrial manufacturing criteria conduct to compounds forming an ideal solid solution. This observation is not surprising, because all the studies of the $(U_{1-y}, Ce_y)O_{2.00}$ phase diagram lead to the same conclusion, irrespective of the manufacturing process.

Table 5
$(U_{1-y}, Ce_y)O_2$ best fit results for the first three coordination shells obtained at the uranium L_{III} edge

Cerium concentration (at.%)	First shell			Second shell						Third shell		
	U–O			U–U			U–Ce			U–O		
	N	R (Å)	$\sigma^2 \times 10^3$ (Å^2)	N	R (Å)	$\sigma^2 \times 10^3$ (Å^2)	N	R (Å)	$\sigma^2 \times 10^3$ (Å^2)	N	R (Å)	$\sigma^2 \times 10^3$ (Å^2)
5	8.0(2)	2.364(5)	5.6(4)	11.4(2)	3.877(9)	3.9(2)	0.7(3)	3.88(2)	8(5)	24(2)	4.52(1)	6(1)
10	8.0(2)	2.365(6)	6.5(5)	10.8(2)	3.873(5)	4.4(3)	1.2(2)	3.87(2)	8(3)	24(2)	4.51(1)	8(1)
12	8.1(2)	2.367(8)	6.4(6)	10.6(2)	3.861(8)	4.3(3)	1.4(2)	3.86(3)	12(3)	24(2)	4.51(4)	9(1)
18	8.1(2)	2.363(8)	7.4(6)	9.8(2)	3.860(8)	4.5(4)	2.1(2)	3.86(3)	8(2)	24(2)	4.50(2)	8(1)
25	8.0(2)	2.362(8)	6.2(6)	9.0(5)	3.857(9)	4.2(4)	3.0(5)	3.86(4)	8(2)	24(2)	4.51(4)	9(2)
50	8.0(2)	2.350(5)	7.2(6)	6.3(3)	3.847(9)	4.2(4)	5.7(3)	3.85(1)	6(2)	24(2)	4.49(1)	9(1)

Table 6
$(U_{1-y}, Ce_y)O_2$ best fit results for the first three coordination shells obtained at the cerium K-edge for 5 and 10 at.% samples and L_I edge for 50 at.% sample

Cerium concentration (at.%)	First shell			Second shell						Third shell		
	Ce–O			Ce–U			Ce–Ce			Ce–O		
	N	R (Å)	$\sigma^2 \times 10^3$ (Å^2)	N	R (Å)	$\sigma^2 \times 10^3$ (Å^2)	N	R (Å)	$\sigma^2 \times 10^3$ (Å^2)	N	R (Å)	$\sigma^2 \times 10^3$ (Å^2)
5	8.0(2)	2.371(7)	2.3(4)	12.0(2)	3.87(1)	1.9(2)				24(2)	4.53(2)	7(3)
10	8.0(2)	2.364(7)	2.2(4)	12.0(2)	3.87(1)	1.6(2)				24(2)	4.51(2)	4(2)
50	8.1(5)	2.353(4)	2.8(5)	6.0(2)	3.85(1)	3.3(5)	6.0(2)	3.85(2)	3.8(7)	25(2)	4.51(2)	7(2)

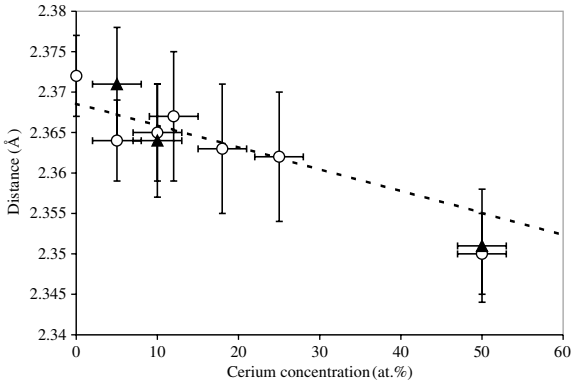

Fig. 4. Metal–oxygen bond distance of the first coordination shell in $(U_{1-y}, Ce_y)O_2$. Open circles and black triangles correspond to uranium and cerium measurements, respectively. Vegard's law is indicated as dashed line.

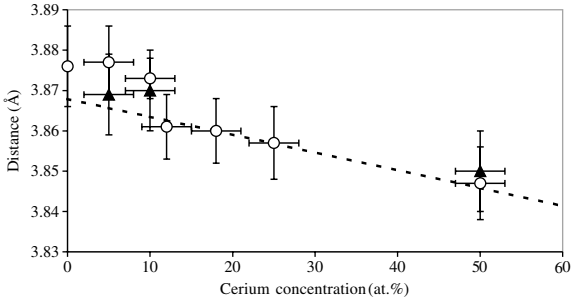

Fig. 5. Metal–uranium bond distance of the second coordination shell in $(U_{1-y}, Ce_y)O_2$. Open circles and black triangles correspond to uranium and cerium measurements, respectively. Vegard's law is indicated as dashed line.

In spite of experimental error margins on the determination of interatomic distances much larger than the ones obtained by X-ray or neutron diffraction, EXAFS leads to the same result, which shows the absence of an inhomogeneous cerium aggregate distribution. Indeed, considering the macroscopic experimental beam size, this technique allows to measure the average distances at a local range in the sample. Moreover, because of the Gaussian approximation of the Debye–Waller factors, the EXAFS appears to be very sensitive to the distribution symmetry of the distances around the given average position during the refinement. No distance was required in addition to those relative to the ideal solid solution. No third cumulant was required in the fitting procedure. This proves on an atomic scale the absence of cerium oxide clusters in the samples studied.

No hyperstoichiometric oxygen defects are revealed whether around uranium or cerium atoms. Indeed, to verify it, hyperstoichiometric uranium oxide samples were also analysed at uranium L_{III} edge. As an example,

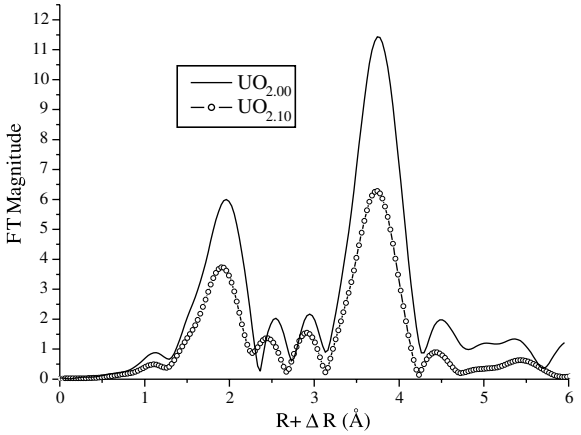

Fig. 6. Comparison of the uranium L_{III}-edge Fourier transforms of $UO_{2.00}$ and $UO_{2.10}$.

we represented in Fig. 6, the Fourier Transform of the reference $UO_{2.00}$ and of a sample $UO_{2.10}$. The overall structure of the FT is always characterised by the presence of two intense peaks. The main difference appears in the FT global intensity which varies drastically. Indeed, the FT total intensity is reduced by 40% from $UO_{2.00}$ to $UO_{2.10}$. As we can see in Fig. 3, the intensity of the first peak, corresponding to the U–O distance, is the same in all $(U_{1-y}, Ce_y)O_2$ samples. Moreover, in the fits, the first coordination sphere is perfectly reproduced by only one U–O distance.

The presence of oxygen defects in uranium dioxide is characterised by oxygen ions in two positions very close to the octahedral vacancies of the face centred cubic structure [16,17] and by the appearance of vacancies in the regular anion lattice. These two positions called O′ and O″ are localised at $(0.5, 0.38, 0.38)$ and $(0.38, 0.38, 0.38)$. The presence of these defects implies the appearance of new U–O distances and the modification of the coordination number. Being too close, it is not possible to introduce successively these distances in the fit as independent shells. Generally speaking, such a distribution of distances implies the introduction of a third or even a fourth cumulant in the fitting procedure to obtain physical values. Excellent fits resulted from the use of a single U–O distance thus proving the absence of the anion defects O′ and O″.

7. Conclusion

A study of the $(U_{1-y}, Ce_y)O_2$ compounds has been performed by EXAFS at the uranium L_{III} and at the cerium K and L_I edges. The absence of cerium oxide clusters or oxygen point defects in our samples is proven. The technique used therefore corroborates on an atomic level that uranium and cerium dioxides form

an ideal solid solution for cerium concentrations ranging between 0 and 50 at.%. Studies on MOX fuel using the same methodology are in progress and will be published in a near future. Other experiments coupled with ab initio calculations are also performed to determine the localisation of elements implanted in fuel to simulate fission product behaviour.

Acknowledgement

Very fruitful discussions with Dr Lionel Desgranges are greatly acknowledged.

References

[1] M. Beauvy, J. Nucl. Mater. 188 (1992) 232.
[2] T.L. Markin, R.S. Street, J. Inorg. Nucl. Chem. 32 (1970) 59.
[3] R. Lorenzelli, B. Touzelin, J. Nucl. Mater. 95 (1980) 290.
[4] Y. Nagai, T. Yamamoto, T. Tanaka, S. Yoshida, T. Nonaka, T. Okamoto, A. Suda, M. Sugiura, J. Synchr. Rad. 8 (2001) 616.
[5] D.J. Jones, J. Roziere, G.C. Allen, P.A. Tempest, J. Chem. Phys 84 (1986) 6075.
[6] F. Jollet, T. Petit, S. Gota, N. Thromat, M. Gautier-Soyer, A. Pasturel, J. Phys.: Condens. Matter 9 (1997) 9393.
[7] Z.Y. Wu, F. Jollet, S. Gota, N. Thromat, M. Gautier-Soyer, T. Petit, J. Phys.: Condens. Matter 11 (1999) 7185.
[8] T. Reich, G. Bernhard, G. Geipel, H. Funke, C. Hennig, A. Rossberg, W. Matz, N. Schell, H. Nitsche, Radiochim. Acta 88 (2000) 633.
[9] E. Fonda, D. Andreatta, P.E. Colavita, G. Vlaic, J. Synchr. Rad. 6 (1999) 34.
[10] S. Pascarelli, F. Boscherini, F. D'Acapito, J. Hrdy, C. Meneghini, S. Mobilio, J. Synchr. Rad. 3 (1996) 147.
[11] K. Yamada, S. Yamanaka, T. Nakagawa, M. Uno, M. Katsura, J. Nucl. Mater. 247 (1997) 289.
[12] L. Tröger, D. Arvanitis, K. Baberschke, H. Michaelis, U. Grimm, E. Zschech, Phys. Rev. B 46 (1992) 3283.
[13] E.A. Stern, M. Newville, B. Ravel, Y. Yacoby, D. Haskel, Physica B 209 (1995) 117.
[14] M. Newville, J. Synchr. Rad. 8 (2001) 100.
[15] A.L. Ankudinov, B. Ravel, J.J. Rehr, S.D. Conradson, Phys. Rev. B 58 (1998) 7565.
[16] A.D. Murray, B.T.M. Willis, J. Solid State Chem. 84 (1990) 52.
[17] B.T.M. Willis, Acta Cryst. A 34 (1978) 88.